

Scattering by a three-dimensional object composed of the simplest Lorentz-nonreciprocal medium

Hamad M. Alkhoori,¹ Akhlesh Lakhtakia,² James K. Breakall,¹ and Craig F. Bohren³

¹Department of Electrical Engineering, The Pennsylvania State University, University Park, Pennsylvania 16802, USA

²Department of Engineering Science and Mechanics, The Pennsylvania State University, University Park, Pennsylvania 16802, USA

³Department of Meteorology, The Pennsylvania State University, University Park, Pennsylvania 16802, USA

Abstract

The simplest Lorentz-nonreciprocal medium has the constitutive relations ($\mathbf{D} = \varepsilon_0 \mathbf{E} - \mathbf{\Gamma} \times \mathbf{H}$ and $\mathbf{B} = \mu_0 \mathbf{H} + \mathbf{\Gamma} \times \mathbf{E}$). Scattering by a three-dimensional object composed of this medium was investigated using the extended boundary condition method. Scattering by this object in free space must be attributed to non-zero $\mathbf{\Gamma} = |\mathbf{\Gamma}|$. The differential scattering efficiency is immune to the transformation of the incident toroidal electric field phasor into a poloidal electric field phasor, or *vice versa*, and a consequence of this source-invariance is the polarization-state invariance of the differential scattering efficiency when the irradiating field is a plane wave. Both the total scattering and forward-scattering efficiencies of an ellipsoid composed of the simplest Lorentz-nonreciprocal medium are maximum when the plane wave is incident in a direction coparallel (but not antiparallel) to $\mathbf{\Gamma}$, and the backscattering efficiency is minimum when $\mathbf{\Gamma}$ is parallel to the incidence direction. The total scattering and the forward-scattering efficiencies are maximum when the incidence direction is parallel to the largest semi-axis of the ellipsoid if the incidence direction is coparallel (but not antiparallel) to $\mathbf{\Gamma}$. Lorentz nonreciprocity in an object is thus intimately connected to the shape of that object in affecting the scattered field.

1 Introduction

A remarkable feature of 21st-century electromagnetics is the diversity of linear materials in which electromagnetic phenomena are being investigated. These materials can be isotropic, biisotropic, anisotropic or bianisotropic [1, 2, 3, 4]. These materials can be reciprocal or nonreciprocal in the Lorentz sense [5]. Natural examples of some types of these materials may not be known or are very uncommon, but can be engineered [6, 7, 8] as composite materials [9, 10].

Several composite materials have been proposed to replicate certain characteristics of relativistic spacetime [11, 12, 13, 14, 15, 16, 17], based on a theorem of Plébanski [18] according to which relativistic spacetime can be replaced by a bianisotropic continuum. This continuum may exhibit the magnetoelectric [19] effect in a Lorentz-nonreciprocal sense [20]. Suppose that relativistic spacetime is described by the gravitational metric $g_{\alpha\beta}$, $\alpha \in \{0, 1, 2, 3\}$ and $\beta \in \{0, 1, 2, 3\}$, with $(+, -, -, -)$ as its signature. We can then define a dyadic $\underline{\gamma}$ and a vector $\mathbf{\Gamma}$ with components $\gamma_{\ell m} = -(-\bar{g})^{1/2} g^{\ell m} / g_{00}$ and $\Gamma_\ell = c_0^{-1} g_{0\ell} / g_{00}$, $\ell \in \{1, 2, 3\}$ and $m \in \{1, 2, 3\}$, where \bar{g} denotes the determinant of $g_{\alpha\beta}$, $c_0 = 1/\sqrt{\varepsilon_0 \mu_0}$, and ε_0 and μ_0 are the permittivity and the permeability of the gravitationally unaffected free space, respectively. According to the Plébanski theorem, the

constitutive equations of the equivalent bianisotropic continuum are

$$\left. \begin{aligned} \mathbf{D} &= \varepsilon_0 \underline{\underline{\gamma}} \cdot \mathbf{E} - (\mathbf{\Gamma} \times \underline{\underline{I}}) \cdot \mathbf{H} \\ \mathbf{B} &= \mu_0 \underline{\underline{\gamma}} \cdot \mathbf{H} + (\mathbf{\Gamma} \times \underline{\underline{I}}) \cdot \mathbf{E} \end{aligned} \right\}, \quad (1)$$

where $\underline{\underline{I}}$ is the identity dyadic [21].

The vector $\mathbf{\Gamma}$ may be called the magnetoelectric-gyrotropy vector. It has the same role as a bias field in a magnetoplasma or a ferrite [22, 21, 23]; hence the use of the term *gyrotropy*. However, the Plébanski medium specified by Eq. (1) is distinct from magnetoplasmas and ferrites since the gyrotropy in the former case is present in the magnetoelectric dyadics, whereas it is present in the permittivity and permeability dyadics in the latter cases.

Lorentz nonreciprocity is signalled by $\Gamma = |\mathbf{\Gamma}| \neq 0$, because $\mathbf{\Gamma} \times \underline{\underline{I}}$ is an antisymmetric dyadic [5]. In contrast, gravitationally unaffected free space is isotropic and Lorentz reciprocal. Thus, a Lorentz-nonreciprocal counterpart of free space emerges from the spacetime metric [24]

$$[g_{\alpha\beta}] = u^{-1} (u + w_1^2 + w_2^2 + w_3^2)^{-1/4} \begin{bmatrix} 1 & w_1 & w_2 & w_3 \\ w_1 & -u & 0 & 0 \\ w_2 & 0 & -u & 0 \\ w_3 & 0 & 0 & -u \end{bmatrix}, \quad (2)$$

where w_1 , w_2 , and w_3 are the real-valued components of a vector \mathbf{w} and $u > 0$. Then, $\bar{g}u^2 = -1$ and Eqs. (1) hold with $\mathbf{\Gamma} = c_0^{-1} \mathbf{w}$ and $\underline{\underline{\gamma}} = \underline{\underline{I}}$. The constitutive relations of this Lorentz-nonreciprocal medium thus are as follows:

$$\left. \begin{aligned} \mathbf{D} &= \varepsilon_0 \mathbf{E} - (\mathbf{\Gamma} \times \underline{\underline{I}}) \cdot \mathbf{H} \\ \mathbf{B} &= \mu_0 \mathbf{H} + (\mathbf{\Gamma} \times \underline{\underline{I}}) \cdot \mathbf{E} \end{aligned} \right\}. \quad (3)$$

This medium is the *simplest* Lorentz-nonreciprocal medium possible because it differs from free space ($\mathbf{D} = \varepsilon_0 \mathbf{E}$ and $\mathbf{B} = \mu_0 \mathbf{H}$), the reference medium in electromagnetic theory, by a single constitutive scalar: Γ . A bounded object composed of the simplest Lorentz-nonreciprocal medium and suspended in free space can scatter only if $\Gamma \neq 0$.

As the simplest Lorentz-nonreciprocal medium can be transformed into free space by a straightforward transformation of electric and magnetic field phasors [25, 26], simple solutions of the frequency-domain Maxwell equations with Eqs. (3) substituted exist. Accordingly, plane-wave scattering by a sphere composed of the simplest Lorentz-nonreciprocal medium has been theoretically examined [24]. The scattering characteristics depend strongly on the magnitude and direction of $\mathbf{\Gamma}$. The total scattering and forward-scattering efficiencies are more pronounced when $\mathbf{\Gamma}$ is parallel to the propagation direction of the incident plane wave than when it is parallel to either the incident electric field phasor or the incident magnetic field phasor. Also, the backscattering efficiency vanishes when $\mathbf{\Gamma}$ is parallel to the propagation direction of the incident plane wave. But because the scattering object is a sphere, the role of the shape of the object on scattering characteristics could not be unveiled.

Here, we investigate the simultaneous effects of shape and magnetoelectric gyrotropy by formulating and solving the problem of plane-wave scattering by an object composed of the simplest Lorentz-nonreciprocal medium suspended in free space. The extended boundary condition method (EBCM), also called the null-field method and the T-matrix method [27], was adopted to solve the scattering problem. The scattered and internal field phasors were expanded in terms of appropriate vector spherical wavefunctions [27] with unknown expansion coefficients, and the incident

field phasors were similarly expanded but with known expansion coefficients. Application of the Ewald–Oseen extinction theorem and the Huygens principle then yielded a transition matrix to relate the scattered-field coefficients to the incident-field coefficients [28].

The plan of the paper is as follows. The EBCM equations for the chosen scattering problem are presented in Sec. 2. These equations are exploited in Sec. 3 to uncover a source-invariance property of the differential scattering efficiency. Furthermore, we show in Sec. 4 that the plane-wave scattering efficiencies are not affected by the polarization state of the incident plane wave. The plane-wave scattering efficiencies of an ellipsoid composed of the simplest Lorentz-nonreciprocal medium are presented in Sec. 5 in relation to the direction of propagation and the polarization state of the incident plane wave, the shape of the ellipsoid, and the magnetoelectric-gyrotropy vector. Conclusions are summarized in Sec. 6.

An $\exp(-i\omega t)$ dependence on time t is implicit throughout the analysis with $i = \sqrt{-1}$ and ω is the angular frequency. The wavenumber in free space is denoted by $k_0 = \omega/c_0$ and the intrinsic impedance of free space by $\eta_0 = \sqrt{\mu_0/\varepsilon_0}$. Vectors are in boldface, unit vectors are decorated by carets, dyadics are double underlined, and column vectors as well as matrices are enclosed in square brackets.

2 EBCM Equations

Let all space \mathcal{V} be partitioned into two disjoint regions \mathcal{V}_e and \mathcal{V}_i separated by the closed surface \mathcal{S} . Extending to infinity in all directions, the exterior region \mathcal{V}_e is vacuous except that a portion $\mathcal{V}_s \subset \mathcal{V}_e$ is occupied by the source of a time-harmonic electromagnetic field. The interior region \mathcal{V}_i is occupied by the the simplest Lorentz-nonreciprocal medium. The origin of the coordinate system lies in \mathcal{V}_i .

Application of the Ewald–Oseen extinction theorem and the Huygens principle leads to the integral equations [27, 28]

$$\left. \begin{array}{l} \mathbf{E}_{\text{sca}}(\mathbf{r}) \\ -\mathbf{E}_{\text{inc}}(\mathbf{r}) \end{array} \right\} = \iint_{\mathcal{S}} \left\{ -\underline{\underline{G}}^{em}(\mathbf{r}, \mathbf{r}_s) \cdot [\hat{\mathbf{n}}(\mathbf{r}_s) \times \mathbf{E}_{\text{int}}(\mathbf{r}_s)] \right. \\ \left. + \underline{\underline{G}}^{ee}(\mathbf{r}, \mathbf{r}_s) \cdot [\hat{\mathbf{n}}(\mathbf{r}_s) \times \mathbf{H}_{\text{int}}(\mathbf{r}_s)] \right\} d^2r_s, \quad \begin{cases} \mathbf{r} \in \mathcal{V}_e \\ \mathbf{r} \in \mathcal{V}_i \end{cases}. \quad (4)$$

In these equations, $\mathbf{E}_{\text{inc}}(\mathbf{r})$ is the incident electric field phasor, $\mathbf{E}_{\text{sca}}(\mathbf{r})$ is the scattered electric field phasor, $\mathbf{E}_{\text{int}}(\mathbf{r})$ is the internal electric field phasor, $\mathbf{H}_{\text{int}}(\mathbf{r})$ is the internal magnetic field phasor, $\hat{\mathbf{n}}(\mathbf{r}_s)$ is the unit outward normal to \mathcal{S} at $\mathbf{r}_s \in \mathcal{S}$,

$$\underline{\underline{G}}^{em}(\mathbf{r}, \mathbf{r}_s) = -\frac{1}{i\omega\mu_0} \nabla \times \underline{\underline{G}}^{ee}(\mathbf{r}, \mathbf{r}_s), \quad (5)$$

and

$$\underline{\underline{G}}^{ee}(\mathbf{r}, \mathbf{r}_s) = i\omega\mu_0 \left(\underline{\underline{I}} + \frac{\nabla\nabla}{k_0^2} \right) \frac{\exp(ik_0|\mathbf{r} - \mathbf{r}_s|)}{4\pi|\mathbf{r} - \mathbf{r}_s|} \quad (6)$$

is the dyadic Green function for free space [21].

2.1 Incident electric and magnetic field phasors

The incident electric field phasor is expressed as

$$\mathbf{E}_{\text{inc}}(\mathbf{r}) = \lim_{N \rightarrow \infty} \sum_{s \in \{e, o\}} \sum_{n=1}^N \sum_{m=0}^n \{ D_{mn} [A_{smn}^{(1)} \mathbf{M}_{smn}^{(1)}(k_0 \mathbf{r}) + B_{smn}^{(1)} \mathbf{N}_{smn}^{(1)}(k_0 \mathbf{r})] \} \quad (7)$$

and the incident magnetic field phasor as

$$\mathbf{H}_{\text{inc}}(\mathbf{r}) = -\frac{i}{\eta_0} \lim_{N \rightarrow \infty} \sum_{s \in \{e, o\}} \sum_{n=1}^N \sum_{m=0}^n \{ D_{mn} [A_{smn}^{(1)} \mathbf{N}_{smn}^{(1)}(k_0 \mathbf{r}) + B_{smn}^{(1)} \mathbf{M}_{smn}^{(1)}(k_0 \mathbf{r})] \}, \quad (8)$$

where the normalization factor

$$D_{mn} = (2 - \delta_{m0}) \frac{(2n+1)(n-m)!}{4n(n+1)(n+m)!} \quad (9)$$

involves the Kronecker delta $\delta_{mm'}$.

The vector spherical wavefunctions of the first kind, $\mathbf{M}_{smn}^{(1)}(k_0 \mathbf{r})$ and $\mathbf{N}_{smn}^{(1)}(k_0 \mathbf{r})$, are available in standard texts [29, 30, 31], the index n denoting the order of the spherical Bessel function $j_n(k_0 r)$ appearing in those wavefunctions. The index n is restricted to $[1, N]$ where N is sufficiently large for acceptable convergence and the limit on the right sides of Eqs. (7) and (8) is not used. The vector spherical wavefunctions also contain the associated Legendre function $P_n^m(\cos \theta)$ of order n and degree m , and the index s stands for either even (e) or odd (o) parity.

The column vectors $[A^{(1)}]$ and $[B^{(1)}]$ of the expansion coefficients $A_{smn}^{(1)}$ and $B_{smn}^{(1)}$, respectively, are assumed to be known. An assumption underlying Eqs. (7) and (8) is that the source of the incident field phasors is not affected by scattering by the object.

2.2 Scattered electric and magnetic field phasors

The scattered electric and magnetic field phasors take the form

$$\mathbf{E}_{\text{sca}}(\mathbf{r}) = \lim_{N \rightarrow \infty} \sum_{s \in \{e, o\}} \sum_{n=1}^N \sum_{m=0}^n \{ D_{mn} [A_{smn}^{(3)} \mathbf{M}_{smn}^{(3)}(k_0 \mathbf{r}) + B_{smn}^{(3)} \mathbf{N}_{smn}^{(3)}(k_0 \mathbf{r})] \} \quad (10)$$

and

$$\mathbf{H}_{\text{sca}}(\mathbf{r}) = -\frac{i}{\eta_0} \lim_{N \rightarrow \infty} \sum_{s \in \{e, o\}} \sum_{n=1}^N \sum_{m=0}^n \{ D_{mn} [A_{smn}^{(3)} \mathbf{N}_{smn}^{(3)}(k_0 \mathbf{r}) + B_{smn}^{(3)} \mathbf{M}_{smn}^{(3)}(k_0 \mathbf{r})] \}. \quad (11)$$

The vector spherical wavefunctions of the third kind [29, 30, 31], $\mathbf{M}_{smn}^{(3)}(k_0 \mathbf{r})$ and $\mathbf{N}_{smn}^{(3)}(k_0 \mathbf{r})$, involve the spherical Hankel function $h_n^{(1)}(k_0 r)$ instead of $j_n(k_0 r)$. The column vectors $[A^{(3)}]$ and

$[B^{(3)}]$ of the expansion coefficients $A_{smn}^{(3)}$ and $B_{smn}^{(3)}$, respectively, are unknown. In a strict sense, Eqs. (10) and (11) hold outside the smallest sphere circumscribing \mathcal{V}_i with its center on the origin of the coordinate system [28].

The scattered electric field phasor can be approximated as [32, 33]

$$\mathbf{E}_{\text{sca}}(r, \theta, \phi) \approx \mathbf{F}_{\text{sca}}(\theta, \phi) \frac{\exp(ik_0 r)}{r} \quad (12)$$

as $k_0 r \rightarrow \infty$, where [34]

$$\mathbf{F}_{\text{sca}}(\theta, \phi) = \frac{1}{k_0} \lim_{N \rightarrow \infty} \sum_{s \in \{e, o\}} \sum_{n=1}^N \sum_{m=0}^n \left\{ (-i)^n D_{mn} \sqrt{n(n+1)} \right. \\ \left. \left[-i A_{smn}^{(3)} \mathbf{C}_{smn}(\theta, \phi) + B_{smn}^{(3)} \hat{\mathbf{r}} \times \mathbf{C}_{smn}(\theta, \phi) \right] \right\} \quad (13)$$

involves

$$\mathbf{C}_{smn}(\theta, \phi) = \frac{1}{\sqrt{n(n+1)}} \left[\mp m \frac{P_n^m(\cos \theta)}{\sin \theta} \begin{Bmatrix} \sin(m\phi) \\ \cos(m\phi) \end{Bmatrix} \hat{\boldsymbol{\theta}} \right. \\ \left. - \frac{dP_n^m(\cos \theta)}{d\theta} \begin{Bmatrix} \cos(m\phi) \\ \sin(m\phi) \end{Bmatrix} \hat{\boldsymbol{\phi}} \right], \quad s = \begin{Bmatrix} e \\ o \end{Bmatrix}. \quad (14)$$

The differential scattering efficiency is defined as

$$Q_D(\theta, \phi) = \frac{4}{c^2} |\mathbf{F}_{\text{sca}}(\theta, \phi)|^2, \quad (15)$$

where c is an appropriate linear dimension of the object. The total scattering efficiency is obtained as

$$Q_{\text{sca}} = \frac{1}{(k_0 c)^2} \lim_{N \rightarrow \infty} \sum_{s \in \{e, o\}} \sum_{n=1}^N \sum_{m=0}^n D_{mn} \left[|A_{smn}^{(3)}|^2 + |B_{smn}^{(3)}|^2 \right]. \quad (16)$$

2.3 Internal electric and magnetic field phasors

The electric and magnetic field phasors excited inside the scattering object are represented by [25, 26]

$$\mathbf{E}_{\text{int}}(\mathbf{r}) = \exp(i\omega \boldsymbol{\Gamma} \cdot \mathbf{r}) \lim_{N \rightarrow \infty} \sum_{s \in \{e, o\}} \sum_{n=1}^N \sum_{m=0}^n [b_{smn} \mathbf{M}_{smn}^{(1)}(k_0 \mathbf{r}) \\ + c_{smn} \mathbf{N}_{smn}^{(1)}(k_0 \mathbf{r})], \quad (17)$$

and

$$\mathbf{H}_{\text{int}}(\mathbf{r}) = -\frac{i}{\eta_0} \exp(i\omega \boldsymbol{\Gamma} \cdot \mathbf{r}) \lim_{N \rightarrow \infty} \sum_{s \in \{e, o\}} \sum_{n=1}^N \sum_{m=0}^n [b_{smn} \mathbf{N}_{smn}^{(1)}(k_0 \mathbf{r}) \\ + c_{smn} \mathbf{M}_{smn}^{(1)}(k_0 \mathbf{r})], \quad (18)$$

where the column vectors $[b]$ and $[c]$ comprising the expansion coefficients b_{smn} and c_{smn} , respectively, have to be determined.

2.4 Transition matrix

Equations (7), (8), (10), (11), (17), and (18) are substituted in Eqs. (4) along with the bilinear expansion [26] of $\underline{\underline{G}}^{ee}(\mathbf{r}, \mathbf{r}_s)$ in terms of the vector spherical wavefunctions. After using the orthogonality properties of the vector spherical wavefunctions on unit spheres [30], the incident-field coefficients and the scattered-field coefficients can be related to the tangential components of the electric and magnetic field phasors on the exterior side of S . Standard boundary conditions then connect those tangential components to the internal electric and magnetic field phasors evaluated on the interior side of S [28].

A set of algebraic equations thereby emerges to relate the incident-field coefficients to the internal-field coefficients [27]:

$$\begin{bmatrix} [A^{(1)}] \\ \text{---} \\ [B^{(1)}] \end{bmatrix} = [Y^{(1)}] \begin{bmatrix} [b] \\ \text{---} \\ [c] \end{bmatrix}, \quad (19)$$

in matrix notation. Similarly, a set of algebraic equations emerges to relate the scattered-field coefficients to the internal-field coefficients as follows:

$$\begin{bmatrix} [A^{(3)}] \\ \text{---} \\ [B^{(3)}] \end{bmatrix} = -[Y^{(1)}] \begin{bmatrix} [b] \\ \text{---} \\ [c] \end{bmatrix}. \quad (20)$$

Therefore,

$$\begin{bmatrix} [A^{(3)}] \\ \text{---} \\ [B^{(3)}] \end{bmatrix} = [T] \begin{bmatrix} [A^{(1)}] \\ \text{---} \\ [B^{(1)}] \end{bmatrix}, \quad (21)$$

where

$$[T] = -[Y^{(3)}][Y^{(1)}]^{-1} \quad (22)$$

is the transition matrix.

The matrix $[Y^{(j)}]$, $j \in [1, 3]$, is symbolically written as

$$[Y^{(j)}] = \left(\begin{array}{c|c} I_{smn,s'm'n'}^{(j)} & J_{smn,s'm'n'}^{(j)} \\ \text{---} & \text{---} \\ J_{smn,s'm'n'}^{(j)} & I_{smn,s'm'n'}^{(j)} \end{array} \right). \quad (23)$$

The matrix elements in Eq. (23) are surface integrals given by

$$\begin{aligned} I_{smn,s'm'n'}^{(j)} &= -\frac{ik_0^2}{\pi} \iint_S \left\{ \mathbf{N}_{smn}^{(\ell)}(k_0 \mathbf{r}_s) \cdot [\hat{\mathbf{n}}(\mathbf{r}_s) \times \mathbf{M}_{s'm'n'}^{(1)}(k_0 \mathbf{r}_s)] \right. \\ &\quad \left. + \mathbf{M}_{smn}^{(\ell)}(k_0 \mathbf{r}_s) \cdot [\hat{\mathbf{n}}(\mathbf{r}_s) \times \mathbf{N}_{s'm'n'}^{(1)}(k_0 \mathbf{r}_s)] \right\} \\ &\quad \times \exp(i\omega \mathbf{\Gamma} \cdot \mathbf{r}_s) d^2 r_s \end{aligned} \quad (24)$$

and

$$\begin{aligned}
J_{smn,s'm'n'}^{(j)} &= -\frac{ik_0^2}{\pi} \iint_S \left\{ \mathbf{N}_{smn}^{(\ell)}(k_0\mathbf{r}_s) \cdot [\hat{\mathbf{n}}(\mathbf{r}_s) \times \mathbf{N}_{s'm'n'}^{(1)}(k_0\mathbf{r}_s)] \right. \\
&\quad \left. + \mathbf{M}_{smn}^{(\ell)}(k_0\mathbf{r}_s) \cdot [\hat{\mathbf{n}}(\mathbf{r}_s) \times \mathbf{M}_{s'm'n'}^{(1)}(k_0\mathbf{r}_s)] \right\} \\
&\quad \times \exp(i\omega\boldsymbol{\Gamma} \cdot \mathbf{r}_s) d^2r_s.
\end{aligned} \tag{25}$$

The symmetries

$$\left. \begin{aligned}
I_{smn,s'm'n'}^{(j)} &= -I_{s'm'n',smn}^{(j)} \\
J_{smn,s'm'n'}^{(j)} &= -J_{s'm'n',smn}^{(j)}
\end{aligned} \right\} \tag{26}$$

should be used to increase computational speed.

3 Toroidal-poloidal source invariance of differential scattering efficiency

A remarkable feature of an object composed of the simplest Lorentz-nonreciprocal medium becomes evident on exchanging the column vectors $[A^{(1)}]$ and $[B^{(1)}]$ on the left side of Eq. (19). This equation remains invariant if the column vectors $[b]$ and $[c]$ on its right side are interchanged as well. If the column vectors $[A^{(3)}]$ and $[B^{(3)}]$ on the left side of Eq. (20) are also interchanged at the same time, then Eqs. (20) and (21) also remain unchanged.

This property leads to the toroidal-poloidal source invariance of the differential scattering efficiency of any object composed of the simplest Lorentz-nonreciprocal medium as follows. Let the incident electric field phasors from sources I and II be given by

$$\begin{aligned}
\mathbf{E}_{\text{inc}}^I(\mathbf{r}) &= \lim_{N \rightarrow \infty} \sum_{s \in \{e,o\}} \sum_{n=1}^N \sum_{m=0}^n \left\{ D_{mn} [A_{smn}^{(1)} \mathbf{M}_{smn}^{(1)}(k_0\mathbf{r}) \right. \\
&\quad \left. + B_{smn}^{(1)} \mathbf{N}_{smn}^{(1)}(k_0\mathbf{r}) \right\}
\end{aligned} \tag{27}$$

and

$$\begin{aligned}
\mathbf{E}_{\text{inc}}^{II}(\mathbf{r}) &= \lim_{N \rightarrow \infty} \sum_{s \in \{e,o\}} \sum_{n=1}^N \sum_{m=0}^n \left\{ D_{mn} [B_{smn}^{(1)} \mathbf{M}_{smn}^{(1)}(k_0\mathbf{r}) \right. \\
&\quad \left. + A_{smn}^{(1)} \mathbf{N}_{smn}^{(1)}(k_0\mathbf{r}) \right\}
\end{aligned} \tag{28}$$

Then, the corresponding scattered electric field phasors must be

$$\begin{aligned}
\mathbf{E}_{\text{sca}}^I(\mathbf{r}) &= \lim_{N \rightarrow \infty} \sum_{s \in \{e,o\}} \sum_{n=1}^N \sum_{m=0}^n \left\{ D_{mn} [A_{smn}^{(3)} \mathbf{M}_{smn}^{(3)}(k_0\mathbf{r}) \right. \\
&\quad \left. + B_{smn}^{(3)} \mathbf{N}_{smn}^{(3)}(k_0\mathbf{r}) \right\}
\end{aligned} \tag{29}$$

and

$$\begin{aligned}
\mathbf{E}_{\text{sca}}^{II}(\mathbf{r}) &= \lim_{N \rightarrow \infty} \sum_{s \in \{e,o\}} \sum_{n=1}^N \sum_{m=0}^n \left\{ D_{mn} [B_{smn}^{(3)} \mathbf{M}_{smn}^{(3)}(k_0\mathbf{r}) \right. \\
&\quad \left. + A_{smn}^{(3)} \mathbf{N}_{smn}^{(3)}(k_0\mathbf{r}) \right\}.
\end{aligned} \tag{30}$$

In consequence, after noting that $\hat{\mathbf{r}} \cdot \mathbf{C}_{smn}(\theta, \phi) \equiv 0$, we see that

$$Q_D^I(\theta, \phi) = Q_D^{II}(\theta, \phi). \quad (31)$$

The vector spherical wave functions $\mathbf{M}_{smn}^{(j)}$ and $\mathbf{N}_{smn}^{(j)}$ are toroidal and poloidal, respectively [35, 36]. The curl of a toroidal/poloidal function is poloidal/toroidal. Accordingly, the source of a toroidal/poloidal electric field phasor is also the source of a poloidal/toroidal magnetic field phasor. Equation (31) demonstrates that the transformation of a source of a toroidal electric field phasor to the source of a poloidal electric field phasor, or *vice versa*, does not affect the differential scattering efficiency of an object composed of the simplest Lorentz-nonreciprocal medium. This toroidal-poloidal source invariance extends to the total scattering efficiency Q_{sca} .

4 Polarization-state invariance of plane-wave scattering efficiencies

As a corollary of the toroidal-poloidal source invariance of the differential scattering efficiency of any object composed of the simplest Lorentz-nonreciprocal medium, the polarization-state invariance holds for the plane-wave scattering efficiencies of that object. The electric field phasor of an incident plane wave is given as

$$\mathbf{E}_{\text{inc}}(\mathbf{r}) = \hat{\mathbf{e}}_{\text{inc}} \exp(i\mathbf{k}_{\text{inc}} \cdot \mathbf{r}), \quad (32)$$

where the unit vector $\hat{\mathbf{e}}_{\text{inc}}$ defines the polarization state and the wave vector

$$\mathbf{k}_{\text{inc}} = k_0(\hat{\mathbf{x}} \sin \theta_{\text{inc}} \cos \phi_{\text{inc}} + \hat{\mathbf{y}} \sin \theta_{\text{inc}} \sin \phi_{\text{inc}} + \hat{\mathbf{z}} \cos \theta_{\text{inc}}), \quad (33)$$

involves the angles $\theta_{\text{inc}} \in [0, \pi]$ and $\phi_{\text{inc}} \in [0, 2\pi)$ that define the incidence direction. The corresponding magnetic field phasor is given as

$$\mathbf{H}_{\text{inc}}(\mathbf{r}) = \frac{\mathbf{k}_{\text{inc}} \times \hat{\mathbf{e}}_{\text{inc}}}{\omega \mu_0} \exp(i\mathbf{k}_{\text{inc}} \cdot \mathbf{r}). \quad (34)$$

The unit vector $\hat{\mathbf{k}}_{\text{inc}} = \mathbf{k}_{\text{inc}}/k_0$ is defined for later convenience and is to be understood as equivalent to the pair $\{\theta_{\text{inc}}, \phi_{\text{inc}}\}$. The expansion coefficients are given by [29, 34]

$$\left. \begin{aligned} A_{smn}^{(1)} &= 4i^n \sqrt{n(n+1)} \hat{\mathbf{e}}_{\text{inc}} \cdot \mathbf{C}_{smn}(\theta_{\text{inc}}, \phi_{\text{inc}}) \\ B_{smn}^{(1)} &= 4i^{n-1} \sqrt{n(n+1)} \hat{\mathbf{e}}_{\text{inc}} \cdot [\hat{\mathbf{k}}_{\text{inc}} \times \mathbf{C}_{smn}(\theta_{\text{inc}}, \phi_{\text{inc}})] \end{aligned} \right\}, \quad (35)$$

For a fixed $\hat{\mathbf{k}}_{\text{inc}}$, $Q_D(\theta, \phi)$ is invariant under a 90° rotation of $\hat{\mathbf{e}}_{\text{inc}}$ about $\hat{\mathbf{k}}_{\text{inc}}$, independently of the shape of the object composed of the simplest Lorentz-nonreciprocal medium. This feature can be derived as follows.

- A 90° rotation of $\hat{\mathbf{e}}_{\text{inc}}$ about $\hat{\mathbf{k}}_{\text{inc}}$ results in the transformation

$$\left\{ A_{smn}^{(1)}, B_{smn}^{(1)} \right\} \rightarrow \left\{ -iB_{smn}^{(1)}, -iA_{smn}^{(1)} \right\}. \quad (36)$$

- Equation (19) then remains unchanged if the transformation

$$\left\{ b_{smn}, c_{smn} \right\} \rightarrow \left\{ -ic_{smn}, -ib_{smn} \right\} \quad (37)$$

is carried out.

- Equation (20) then remains unchanged if the transformation

$$\left\{ A_{smn}^{(3)}, B_{smn}^{(3)} \right\} \rightarrow \left\{ -iB_{smn}^{(3)}, -iA_{smn}^{(3)} \right\} \quad (38)$$

is implemented.

- Use of the transformation of Eq. (38) in Eq. (15) shows that $Q_D(\theta, \phi)$ remains unchanged.

The invariances of the forward-scattering efficiency

$$Q_f = Q_D(\hat{\mathbf{k}}_{\text{inc}}) \quad (39)$$

and the backscattering efficiency

$$Q_b = Q_D(-\hat{\mathbf{k}}_{\text{inc}}) \quad (40)$$

follow from the invariance of $Q_D(\theta, \phi)$, as also does the invariance of Q_{sca} .

Thus, all scattering efficiencies of an object composed of the simplest Lorentz-nonreciprocal medium will not be affected at all by the polarization state of the incident plane wave, regardless of the shape of the object. This is illustrated numerically for an ellipsoid in the next section.

5 Numerical Results and Discussion

The surface \mathcal{S} of the ellipsoid is specified by the position vector

$$\begin{aligned} \mathbf{r}_s(\theta, \phi) &= c\underline{\underline{U}} \cdot [(\hat{\mathbf{x}} \cos \phi + \hat{\mathbf{y}} \sin \phi) \sin \theta + \hat{\mathbf{z}} \cos \theta], \\ \theta &\in [0, \pi], \quad \phi \in [0, 2\pi), \end{aligned} \quad (41)$$

where

$$\underline{\underline{U}} = (a\hat{\mathbf{x}}\hat{\mathbf{x}} + b\hat{\mathbf{y}}\hat{\mathbf{y}}) / c + \hat{\mathbf{z}}\hat{\mathbf{z}} \quad (42)$$

is the shape dyadic. Thus, the ellipsoid has linear dimensions $2a$, $2b$, and $2c$ along the x , y , and z axes, respectively. The shape of the ellipsoid is adequately described by the ratios a/c and b/c . After calculating the transition matrix we determined the differential scattering, total scattering, backscattering, and forward-scattering efficiencies in relation to Γ and k_0c , while keeping the ratios $a/c \neq 1$ and $b/c \neq 1$ fixed.

The calculation of the transition matrix was accomplished on the MathematicaTM platform. We used the Gauss–Legendre quadrature scheme [37, 38] to evaluate the elements of the matrices $[Y^{(1)}]$ and $[Y^{(3)}]$. By testing against known integrals [39], the numbers of nodes for integration over θ and ϕ were chosen to compute the integrals correct to $\pm 0.1\%$ relative error. We used the lower-upper decomposition method to invert $[Y^{(1)}]$ [40, 41, 42]. The value of N was incremented by unity until Q_b converged within a tolerance of $\pm 0.1\%$. The larger the value of Γ , the higher was the value of N required to achieve convergence. The highest value of N is 7 for all results reported here. The Mathematica program was verified by comparing with results available for scattering by a sphere ($a = b = c$) made of the chosen Lorentz-nonreciprocal medium [24]. All results were in complete agreement.

Next, we present numerical results on Q_{sca} , Q_b , Q_f , and Q_D as functions of

- the propagation direction of the incident plane wave ($\hat{\mathbf{k}}_{\text{inc}}$),

- the polarization state of the incident plane wave ($\hat{\mathbf{e}}_{\text{inc}}$),
- the magnitude of the magnetoelectric-gyrotropy vector (Γ),
- the electrical length of the major axis of the ellipsoid (k_0c), and
- the direction of the magnetoelectric-gyrotropy vector ($\hat{\Gamma}$).

Our program accommodates any configuration of the incident plane wave and any orientation of the magnetoelectric-gyrotropy vector. For all of the following results, we set $a/c = 1/2$ and $b/c = 2/3$. Comparison with the results known for a sphere [24] helps us identify the shape effects.

5.1 Effect of Γ

Let us first focus on the effect of Γ on Q_{sca} , Q_{b} , and Q_{f} , while keeping the electrical length k_0c fixed.

Figure 1 shows Q_{sca} vs. $c_0\Gamma \in [0, 0.35]$ for an ellipsoid object composed of the simplest Lorentz-nonreciprocal medium when $k_0c = 3$. These results were calculated for $\hat{\Gamma} \in \{\pm\hat{\mathbf{x}}, \pm\hat{\mathbf{y}}, \pm\hat{\mathbf{z}}\}$, and for all six canonical configurations of the incident plane wave with respect to the semi-axes of the ellipsoid, i.e., $\hat{\mathbf{k}}_{\text{inc}} \in \{\hat{\mathbf{x}}, \hat{\mathbf{y}}, \hat{\mathbf{z}}\}$ and $\hat{\mathbf{e}}_{\text{inc}} \in \{\hat{\mathbf{x}}, \hat{\mathbf{y}}, \hat{\mathbf{z}}\}$ such that $\hat{\mathbf{k}}_{\text{inc}} \perp \hat{\mathbf{e}}_{\text{inc}}$.

For any value of $c_0\Gamma$ in Fig. 1, Q_{sca} is maximum when $\hat{\mathbf{k}}_{\text{inc}} = \hat{\Gamma}$; furthermore, $Q_{\text{sca}}(-\hat{\Gamma}) < Q_{\text{sca}}(\hat{\Gamma})$ then, as becomes increasingly evident with increase of $c_0\Gamma$. Moreover, Q_{sca} is highest when $\hat{\mathbf{k}}_{\text{inc}}$ is parallel to the eigenvector of \underline{U} corresponding to its largest eigenvalue. In contrast, when $\hat{\mathbf{k}}_{\text{inc}} \perp \hat{\Gamma}$, $Q_{\text{sca}}(\hat{\Gamma})$ is almost indistinguishable from $Q_{\text{sca}}(-\hat{\Gamma})$.

Plots of Q_{b} vs. $c_0\Gamma$ are presented in Fig. 2. For all values of $c_0\Gamma$, when $\hat{\mathbf{k}}_{\text{inc}} \perp \hat{\Gamma}$, Q_{b} is the smallest when $\hat{\mathbf{k}}_{\text{inc}}$ is parallel to the eigenvector of \underline{U} corresponding to its largest eigenvalue. Calculations (not shown) for an ellipsoid with $a/c = 2$ and $b/c = 3/2$, for which the eigenvector of \underline{U} corresponding to the largest eigenvalue is $\hat{\mathbf{x}}$, confirms this conclusion. Q_{b} is much smaller when $\hat{\mathbf{k}}_{\text{inc}} \parallel \hat{\Gamma}$ than when $\hat{\mathbf{k}}_{\text{inc}} \perp \hat{\Gamma}$. Furthermore, unlike Q_{sca} , $Q_{\text{b}}(-\hat{\Gamma})$ is almost indistinguishable from $Q_{\text{b}}(\hat{\Gamma})$ when $\hat{\mathbf{k}}_{\text{inc}} \parallel \hat{\Gamma}$.

Finally, plots of Q_{f} vs. $c_0\Gamma$ are presented in Fig. 3. Q_{f} is maximum in this figure when $\hat{\mathbf{k}}_{\text{inc}} = \hat{\Gamma}$; furthermore, $Q_{\text{f}}(-\hat{\Gamma}) < Q_{\text{f}}(\hat{\Gamma})$ then. Moreover, Q_{f} is maximum when $\hat{\mathbf{k}}_{\text{inc}}$ is parallel to the eigenvector of \underline{U} corresponding to its largest eigenvalue, when $\hat{\Gamma} \in \{\hat{\mathbf{x}}, \hat{\mathbf{y}}, \hat{\mathbf{z}}\}$; however, the direction of $\hat{\mathbf{k}}_{\text{inc}}$ relative to the eigenvectors of \underline{U} is virtually inconsequential when $\hat{\Gamma} \in \{-\hat{\mathbf{x}}, -\hat{\mathbf{y}}, -\hat{\mathbf{z}}\}$.

Let us also note that all scattering efficiencies in Figs. 1–3 increase with $c_0\Gamma$. Also, the polarization-state-invariance of all scattering efficiencies is evident in these figures.

5.2 Effect of k_0c

Next, we focus on the effect of k_0c on $Q_{\text{D}}(\theta, \phi)$, Q_{sca} , Q_{b} , and Q_{f} , while keeping the magnitude Γ of the magnetoelectric-gyrotropy vector $\mathbf{\Gamma}$ fixed.

The differential scattering efficiency $Q_{\text{D}}(\theta, \phi)$ is shown in Fig. 4 as a function of θ for $\phi = 0^\circ$ when $\hat{\mathbf{k}}_{\text{inc}} = \hat{\mathbf{z}}$, $\hat{\mathbf{e}}_{\text{inc}} \in \{\hat{\mathbf{x}}, \hat{\mathbf{y}}\}$, and $\hat{\Gamma} \in \{\hat{\mathbf{x}}, \hat{\mathbf{y}}, \hat{\mathbf{z}}\}$. Recall that $Q_{\text{D}}(\theta, \phi)$ has to be independent of $\hat{\mathbf{e}}_{\text{inc}}$, in accord with Sec. 4. Most importantly, as k_0c increases, lobes form in the curves of $Q_{\text{D}}(\theta, 0^\circ)$ regardless of $\hat{\Gamma}$, the same conclusion emerging from similar curves (not shown) for other values of ϕ .

Figure 5 shows Q_{sca} as a function of k_0c for an ellipsoid composed of the simplest Lorentz-nonreciprocal medium with $c_0\Gamma = 0.25$, when $\hat{\Gamma} = \pm\hat{\mathbf{k}}_{\text{inc}}$ and $\hat{\mathbf{k}}_{\text{inc}} \in \{\hat{\mathbf{x}}, \hat{\mathbf{y}}, \hat{\mathbf{z}}\}$. As k_0c increases, the excess of Q_{sca} for $\hat{\Gamma} = \hat{\mathbf{k}}_{\text{inc}}$ over Q_{sca} for $\hat{\Gamma} = -\hat{\mathbf{k}}_{\text{inc}}$ becomes evident. Furthermore, this excess is maximum (minimum) when $\hat{\Gamma}$ is parallel to the eigenvector of \underline{U} corresponding to the largest (smallest) eigenvalue. The same observations were made for Q_f (not shown). The excess of Q_b for $\hat{\Gamma} = \hat{\mathbf{k}}_{\text{inc}}$ over Q_b for $\hat{\Gamma} = -\hat{\mathbf{k}}_{\text{inc}}$ was very tiny, however (not shown).

Figure 6 shows plots of Q_{sca} vs. k_0c for an ellipsoid composed of the simplest Lorentz-nonreciprocal medium with $c_0\Gamma = 0.25$ when $\hat{\mathbf{k}}_{\text{inc}} \in \{\hat{\mathbf{x}}, \hat{\mathbf{y}}, \hat{\mathbf{z}}\}$ and $\hat{\Gamma} \in \{\hat{\mathbf{x}}, \hat{\mathbf{y}}, \hat{\mathbf{z}}\}$. For any value of k_0c , Q_{sca} is highest when $\hat{\Gamma} = \hat{\mathbf{k}}_{\text{inc}}$; furthermore, Q_{sca} is less for $\hat{\Gamma} = -\hat{\mathbf{k}}_{\text{inc}}$, which follows from Fig. 5. Additionally, Q_{sca} is maximum when $\hat{\mathbf{k}}_{\text{inc}}$ is parallel to the eigenvector of \underline{U} corresponding to its largest eigenvalue.

Figure 7 shows Q_b vs. k_0c for an ellipsoid composed of the simplest Lorentz-nonreciprocal medium with $c_0\Gamma = 0.25$ when $\hat{\mathbf{k}}_{\text{inc}} \in \{\hat{\mathbf{x}}, \hat{\mathbf{y}}, \hat{\mathbf{z}}\}$ and $\hat{\Gamma} \in \{\hat{\mathbf{x}}, \hat{\mathbf{y}}, \hat{\mathbf{z}}\}$. As mentioned in Sec. 5.A, $Q_b(-\hat{\Gamma})$ is almost indistinguishable from $Q_b(\hat{\Gamma})$ when $\hat{\mathbf{k}}_{\text{inc}} \parallel \hat{\Gamma}$. We conclude from Fig. 7 that Q_b is the minimum when either $\hat{\Gamma} = \hat{\mathbf{k}}_{\text{inc}}$ or $\hat{\Gamma} = -\hat{\mathbf{k}}_{\text{inc}}$, regardless of k_0c , for a fixed $\hat{\mathbf{k}}_{\text{inc}}$. In this trend, Q_b differs from Q_{sca} .

Figure 8 is the counterpart of Fig. 7 for Q_f . Like Q_{sca} , Q_f is maximum when $\hat{\Gamma} = \hat{\mathbf{k}}_{\text{inc}}$, and is less when $\hat{\Gamma} = -\hat{\mathbf{k}}_{\text{inc}}$ based on an argument similar to that of Fig. 5 but for Q_f (not shown). Moreover, Q_f is maximum when $\hat{\mathbf{k}}_{\text{inc}}$ is parallel to the eigenvector of \underline{U} corresponding to its largest eigenvalue.

6 Concluding Remarks

The medium described by Eqs. (1) is the simplest Lorentz-nonreciprocal medium, differing from the free space by virtue of a non-null magnetoelectric-gyrotropy vector $\mathbf{\Gamma}$. When an object composed of this medium suspended in free space is irradiated by electromagnetic fields from a source, the differential scattering efficiency is immune to the transformation of the incident toroidal electric field phasor into a poloidal electric field phasor, or *vice versa*. Of course, the magnetic field phasor accompanying a toroidal/poloidal electric field phasor is poloidal/toroidal, by virtue of the Faraday equation. This toroidal-poloidal source-invariance is also exhibited by the total scattering efficiency.

A consequence of the toroidal-poloidal source-invariance of the differential scattering efficiency is the polarization-state invariance of the differential scattering efficiency when the irradiating field is a plane wave. As a result, not only the total scattering efficiency but also the forward-scattering and the backscattering efficiencies also exhibit polarization-state invariance.

Numerical results obtained using the extended boundary condition method for plane-wave scattering by an ellipsoid composed of the simplest Lorentz-nonreciprocal medium validated the foregoing conclusions. Furthermore, regardless of the magnitude of the magnetoelectric-gyrotropy vector and the electrical size of the ellipsoid, the total scattering and forward-scattering efficiencies are maximum when the plane wave is incident in a direction that is coparallel (but not antiparallel) to the magnetoelectric-gyrotropy vector, as compared to when the incidence direction is antiparallel or perpendicular to the magnetoelectric-gyrotropy vector. The backscattering efficiency is minimum when the magnetoelectric-gyrotropy vector is parallel to the incidence direction.

When the incidence direction is parallel to the eigenvector of the ellipsoid's shape dyadic corresponding to its largest eigenvalue, the total scattering and the forward-scattering efficiencies are maximum, provided that the incidence direction is coparallel (but not antiparallel) to the

magnetolectric-gyrotropy vector.

As the electrical size of the ellipsoid increases, lobes appear in the curves of the differential scattering efficiency, regardless of the direction of the magnetolectric-gyrotropy vector. Furthermore, the excess of the total scattering and forward-scattering efficiencies when the magnetolectric-gyrotropic vector is coparallel (but not antiparallel) to the incidence direction over when it is antiparallel, increases as the electrical size of the ellipsoid increases. Maximum excess is achieved when the magnetolectric-gyrotropic vector is parallel to the eigenvector of the shape dyadic corresponding to its largest eigenvalue. Thus, the simplest manifestation of Lorentz nonreciprocity in an object is intimately connected to the shape of that object in affecting the scattered field.

Acknowledgment. AL thanks the Charles Godfrey Binder Endowment at Penn State for ongoing support of his research activities.

References

- [1] J. F. Nye, *Physical Properties of Crystals* (Clarendon Press, 1985).
- [2] E. Charney, *The Molecular Basis of Optical Activity* (Krieger, 1985).
- [3] T. G. Mackay and A. Lakhtakia, *Electromagnetic Anisotropy and Bianisotropy* (World Scientific, 2010).
- [4] J. A. Kong, *Electromagnetic Wave Theory* (Wiley, 1986).
- [5] C. M. Krowne, “Electromagnetic theorems for complex anisotropic media,” *IEEE Trans. Antennas Propag.* **32**, 1224–1230 (1984).
- [6] R. Marqués, F. Martín, and M. Sorolla, *Metamaterials with Negative Parameters: Theory, Design, and Microwave Applications* (Wiley, 2007).
- [7] W. Cai and V. Shalaev, *Optical Metamaterials: Fundamentals and Applications* (Springer, 2010).
- [8] I. I. Smolyaninov, *Hyperbolic Metamaterials* (Morgan & Claypool, 2018).
- [9] P. S. Neelakanta, *Handbook of Electromagnetic Materials* (CRC Press, 1995).
- [10] T. G. Mackay and A. Lakhtakia, *Modern Analytical Electromagnetic Homogenization* (Morgan & Claypool, 2015).
- [11] M. Li, R.-X. Miao, and Y. Pang, “Casimir energy, holographic dark energy and electromagnetic metamaterial mimicking de Sitter,” *Phys. Lett. B* **689**, 55–59 (2010).
- [12] M. Li, R.-X. Miao, and Y. Pang, “More studies on metamaterials mimicking de Sitter space,” *Opt. Express* **18**, 9026–9033 (2010).
- [13] T. G. Mackay and A. Lakhtakia, “Towards a realization of Schwarzschild-(anti-)de Sitter spacetime as a particulate metamaterial,” *Phys. Rev. B* **83**, 195424 (2011).

- [14] T. G. Mackay and A. Lakhtakia, “Towards a metamaterial simulation of a spinning cosmic string,” *Phys. Lett. A* **374**, 2305–2308 (2010).
- [15] R.-X. Miao, R. Zheng, and M. Li, “Metamaterials mimicking dynamic spacetime, D-brane and noncommutativity in string theory,” *Phys. Lett. B* **696**, 550–555 (2011).
- [16] T. G. Mackay and A. Lakhtakia, “Towards a piecewise-homogeneous metamaterial model of the collision of two linearly polarized gravitational plane waves,” *IEEE Trans. Antennas Propagat.* **62**, 6149–6154 (2014).
- [17] D. V. Khveshchenko, “Analogue holographic correspondence in optical metamaterials,” *Europhys. Lett.* **109**, 61001 (2015).
- [18] J. Plébanski, “Electromagnetic waves in gravitational fields,” *Phys. Rev.* **118**, 1396–1408 (1960)
- [19] T. H. O’Dell, *The Electrodynamics of Magneto-electric Media* (North–Holland, 1970).
- [20] T. G. Mackay, A. Lakhtakia, and S. Setiawan, “Gravitation and electromagnetic wave propagation with negative phase velocity,” *New J. Phys.* **7**, 75 (2005).
- [21] H. C. Chen, *Theory of Electromagnetic Waves: A Coordinate-free Approach* (McGraw–Hill, 1985).
- [22] L. B. Felsen and N. Marcuvitz, *Radiation and Scattering of Waves* (IEEE Press, 1994).
- [23] U. S. Inan and M. Golkowski, *Principles of Plasma Physics for Engineering and Scientists* (Cambridge University Press, 2011).
- [24] A. D. U. Jafri and A. Lakhtakia, “Light scattering by magnetoelectrically gyrotropic sphere with unit relative permittivity and relative permeability,” *J. Opt. Soc. Am. A* **31**, 2489–2494 (2014).
- [25] A. Lakhtakia and W. S. Weiglhofer, “On electromagnetic fields in a linear medium with gyrotropic-like magnetoelectric magnetoelectric properties,” *Microw. Opt. Technol. Lett.* **15**, 168–170 (1997).
- [26] M. Faryad and A. Lakhtakia, *Infinite-Space Dyadic Green Functions in Electromagnetism* (Morgan & Claypool, 2018), Secs. 3.13 and 4.1.3.
- [27] P. C. Waterman, “Matrix formulation of electromagnetic scattering,” *Proc. IEEE* **53**, 805–812 (1965).
- [28] A. Lakhtakia, “The Ewald–Oseen extinction theorem and the extended boundary condition method,” in *The World of Applied Electromagnetics*, A. Lakhtakia and C. M. Furse, eds. (Springer, 2018), pp. 481–513.
- [29] P. M. Morse and H. Feshbach, *Methods of Theoretical Physics, Vol. II* (McGraw–Hill, 1953), Chap. 13.
- [30] J. A. Stratton, *Electromagnetic Theory* (McGraw–Hill, 1941), pp. 564–565.

- [31] R. E. Collin, *Field Theory of Guided Waves* (IEEE Press, 1991).
- [32] J. J. Bowman, T. B. A. Senior, and P. L. E. Uslenghi, eds., *Electromagnetic and Acoustic Scattering by Simple Shapes* (North-Holland, 1969).
- [33] C. F. Bohren and D. R. Huffman, *Absorption and Scattering of Light by Small Particles* (Wiley, 1983).
- [34] H. M. Alkhoori, A. Lakhtakia, J. K. Breakall, and C. F. Bohren, “Plane-wave scattering by an ellipsoid composed of an orthorhombic dielectric–magnetic material,” *J. Opt. Soc. Am. A* **35**, 1549–1559 (2018).
- [35] S. Chandrasekhar and P.C. Kendall, “On force-free magnetic fields,” *Astrophys. J.* **126**, 458–461 (1957).
- [36] V. M. Dubovik and S. V. Shabanov, “The gauge invariance, toroid order parameters and radiation in electromagnetic theory,” in *Essays on the Formal Aspects of Electromagnetic Theory*, A. Lakhtakia, ed. (World Scientific, 1993), pp. 399–474.
- [37] Y. Jaluria, *Computer Methods for Engineering* (Taylor & Francis, 1996), Sec. 7.5.3.
- [38] M. N. O. Sadiku, *Numerical Techniques in Electromagnetic with MATLAB* (CRC Press, 2009), Sec. 3.11.5.
- [39] I. S. Gradshteyn and I. M. Ryzhik, *Table of Integrals, Series, and Products* 7th edn. (Academic Press, 2007).
- [40] E. Kreyszig, *Advanced Engineering Mathematics* 10th edn. (Wiley, 2011), Sec. 20.2.
- [41] J. Jin, *The Finite Element Method in Electromagnetics* (IEEE Press, 2014), Sec. 15.1.
- [42] R. Garg, *Analytical and Computational Methods in Electromagnetics* (Artech House, 2008), Sec. A.2.2.

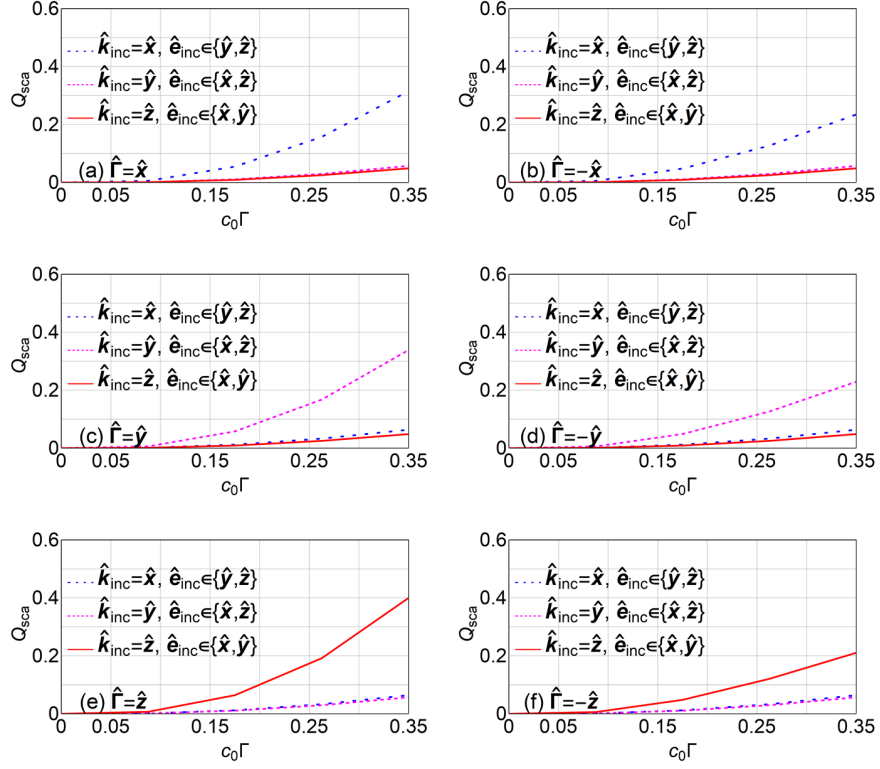


Figure 1: Q_{sca} vs. $c_0\Gamma$ for an ellipsoid composed of the simplest Lorentz-nonreciprocal medium when $k_0c = 3$, $a/c = 1/2$, and $b/c = 2/3$. (a) $\hat{\Gamma} = \hat{x}$, (b) $\hat{\Gamma} = -\hat{x}$, (c) $\hat{\Gamma} = \hat{y}$, (d) $\hat{\Gamma} = -\hat{y}$, (e) $\hat{\Gamma} = \hat{z}$, and (f) $\hat{\Gamma} = -\hat{z}$.

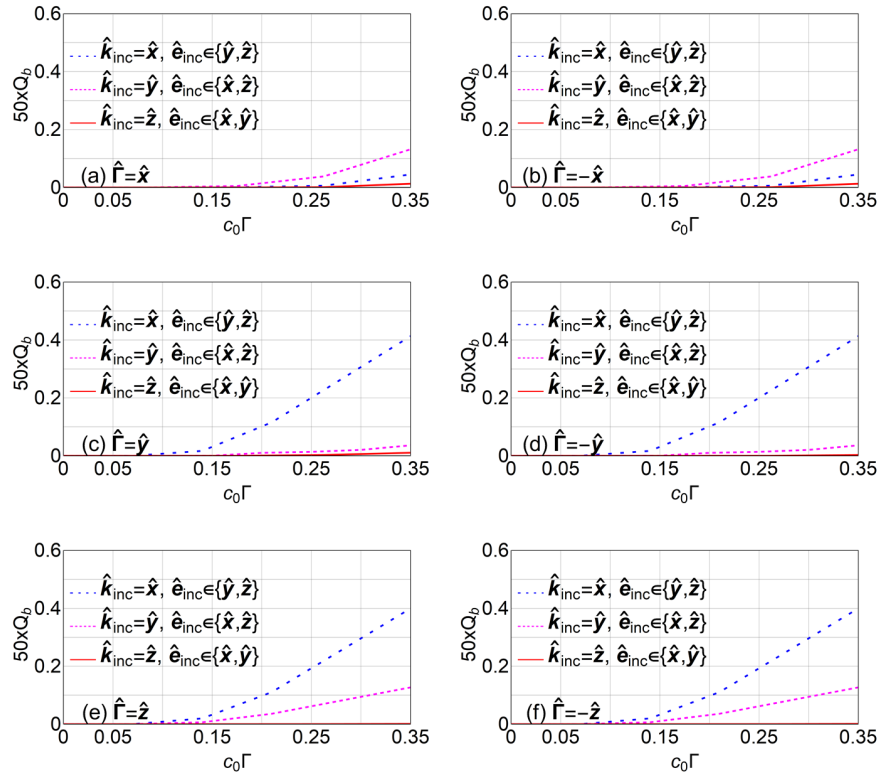


Figure 2: Same as Fig. 1, except for Q_b .

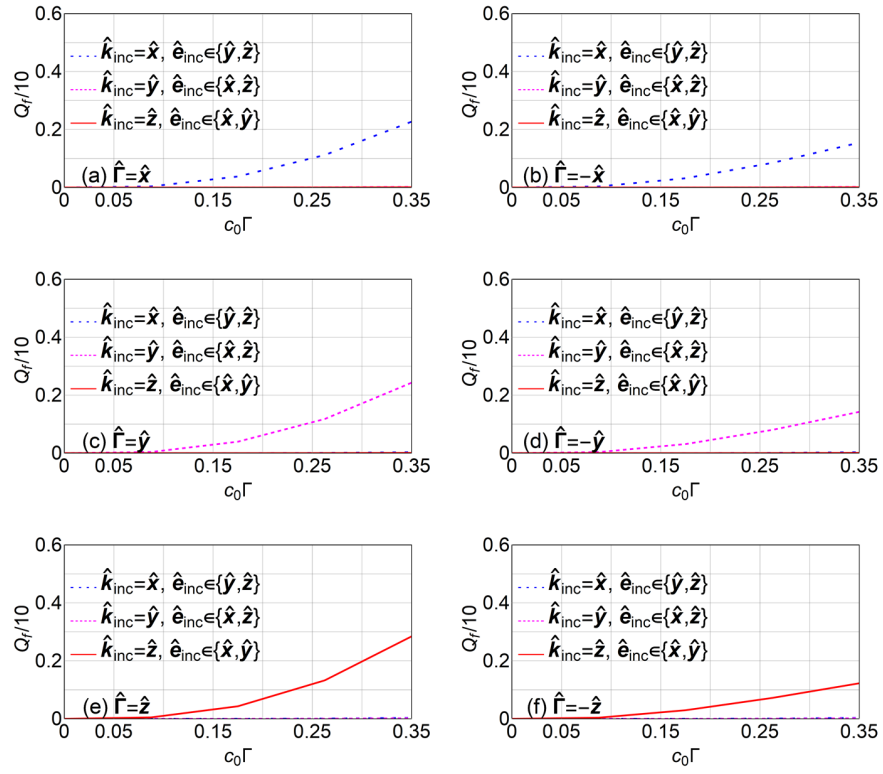


Figure 3: Same as Fig. 1, except for Q_f .

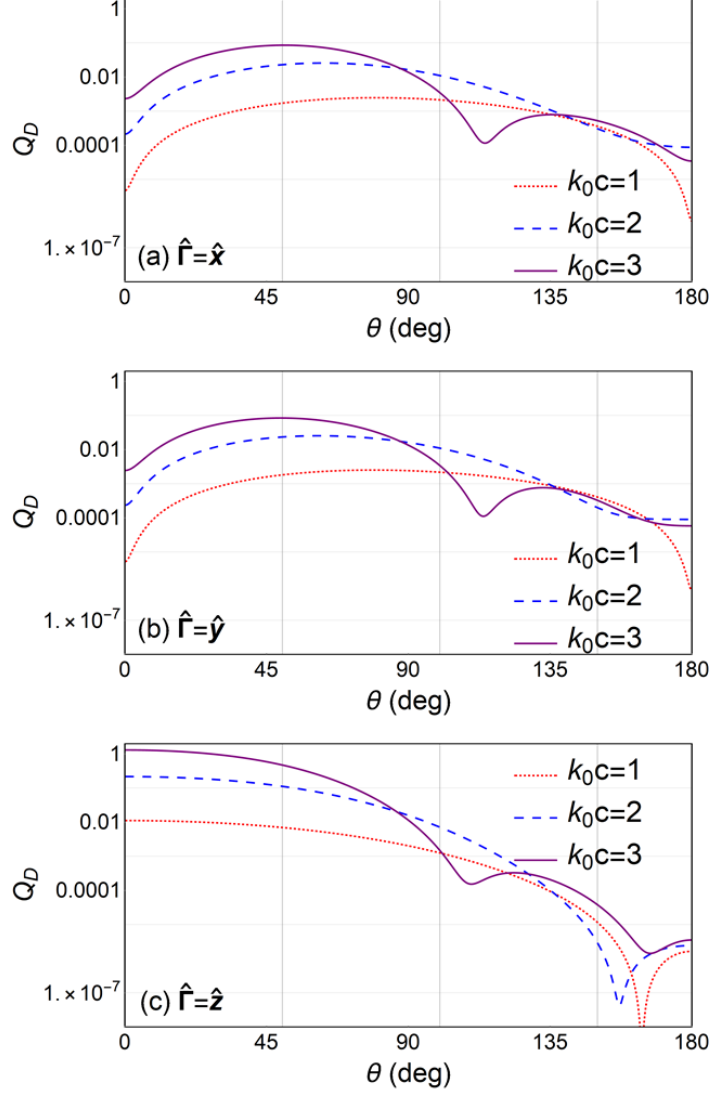


Figure 4: $Q_D(\theta, 0^\circ)$ vs. θ for an ellipsoid composed of the simplest Lorentz-nonreciprocal medium when $k_0 c = 3$, $a/c = 1/2$, $b/c = 2/3$, $c_0 \Gamma = 0.25$, $\hat{\mathbf{k}}_{\text{inc}} = \hat{\mathbf{z}}$, and $\hat{\mathbf{e}}_{\text{inc}} \in \{\hat{\mathbf{x}}, \hat{\mathbf{y}}\}$. The red dotted lines represent $k_0 c = 1$, the blue dashed lines $k_0 c = 2$, and the purple solid lines $k_0 c = 3$. (a) $\hat{\Gamma} = \hat{\mathbf{x}}$, (b) $\hat{\Gamma} = \hat{\mathbf{y}}$, (c) $\hat{\Gamma} = \hat{\mathbf{z}}$.

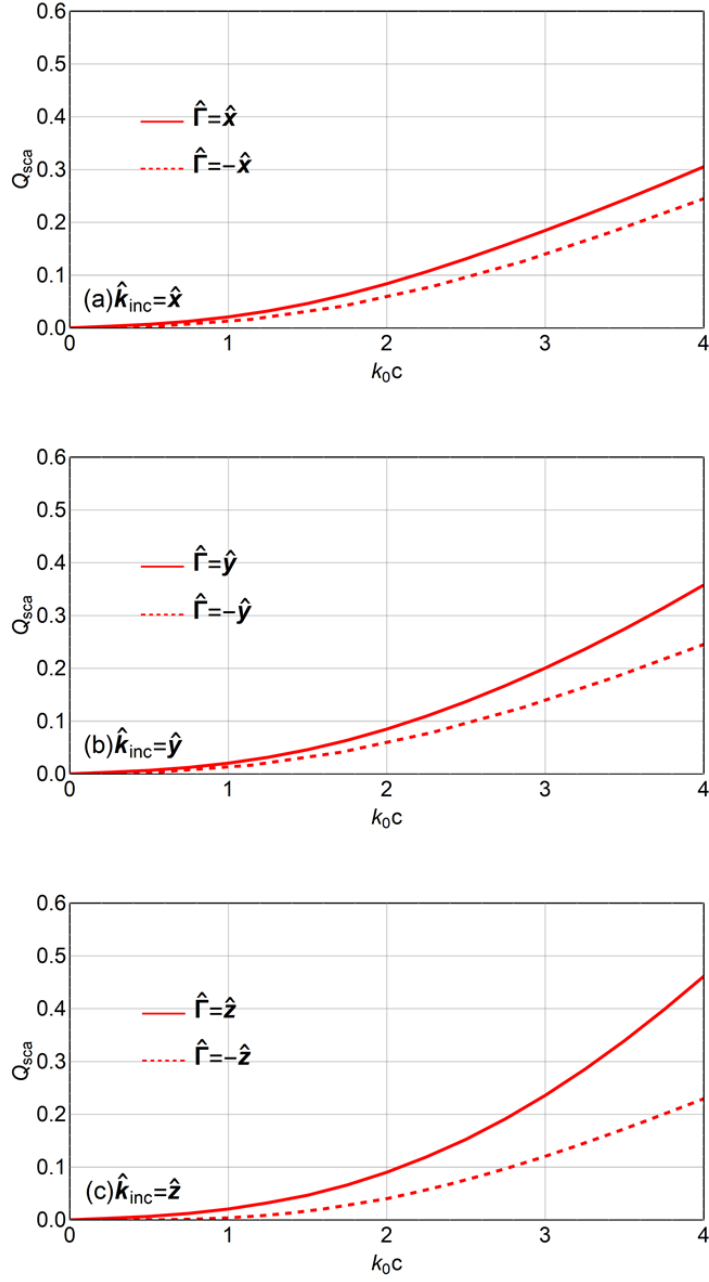


Figure 5: Q_{sca} vs. k_0c for an ellipsoid composed of the simplest Lorentz-nonreciprocal medium when $k_0c = 3$, $a/c = 1/2$, $b/c = 2/3$, $c_0\Gamma = 0.25$, and $\hat{\Gamma} = \pm\hat{\mathbf{k}}_{\text{inc}}$. (a) $\hat{\mathbf{k}}_{\text{inc}} = \hat{\mathbf{x}}$, (b) $\hat{\mathbf{k}}_{\text{inc}} = \hat{\mathbf{y}}$, (c) $\hat{\mathbf{k}}_{\text{inc}} = \hat{\mathbf{z}}$.

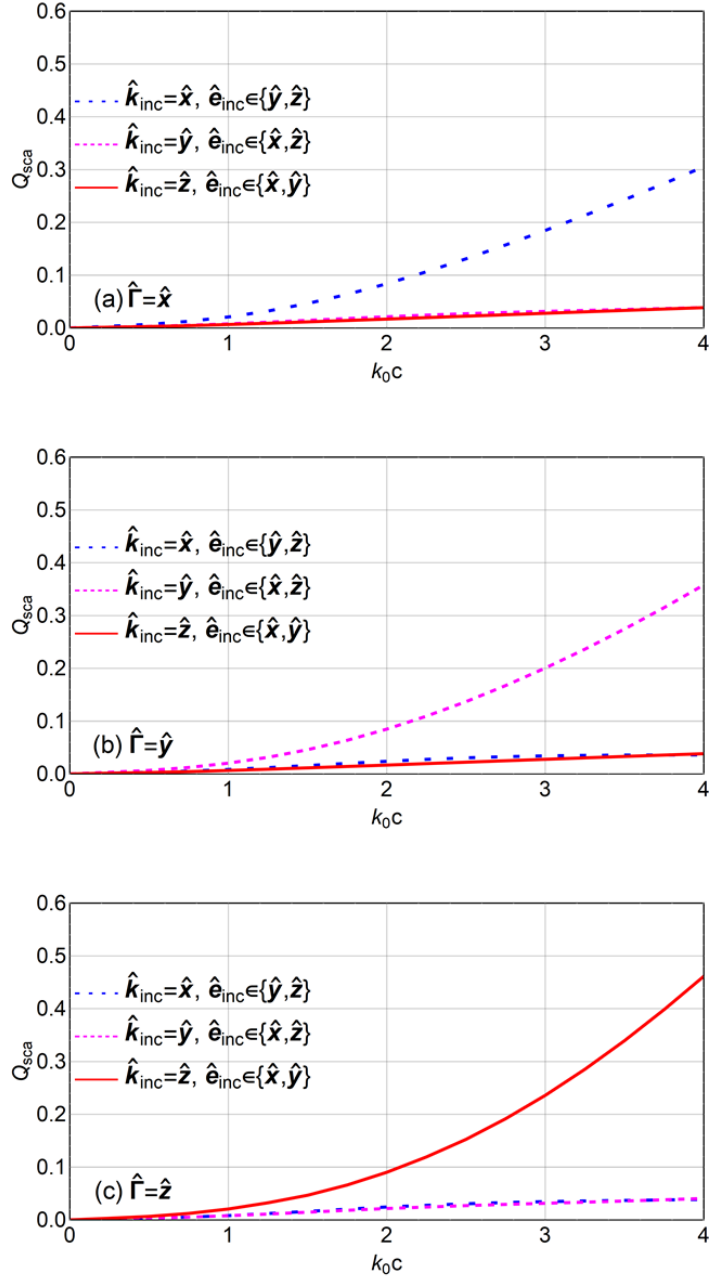


Figure 6: Q_{sca} vs. k_0c for an ellipsoid composed of the simplest Lorentz-nonreciprocal medium when $k_0c = 3$, $a/c = 1/2$, $b/c = 2/3$, $c_0\Gamma = 0.25$, $\hat{\mathbf{k}}_{\text{inc}} \in \{\hat{\mathbf{x}}, \hat{\mathbf{y}}, \hat{\mathbf{z}}\}$, and $\hat{\mathbf{e}}_{\text{inc}} \cdot \hat{\mathbf{k}}_{\text{inc}} = 0$. (a) $\hat{\Gamma} = \hat{\mathbf{x}}$, (b) $\hat{\Gamma} = \hat{\mathbf{y}}$, (c) $\hat{\Gamma} = \hat{\mathbf{z}}$.

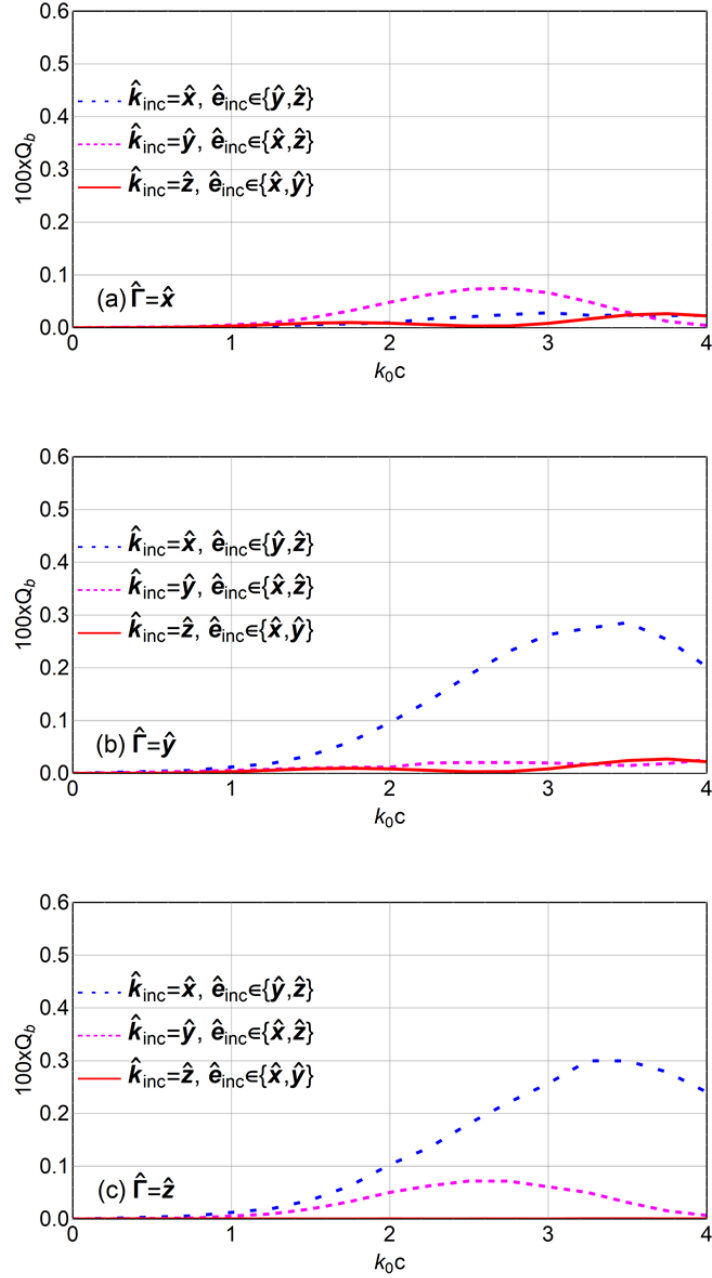


Figure 7: Same as Fig. 6, except for Q_b .

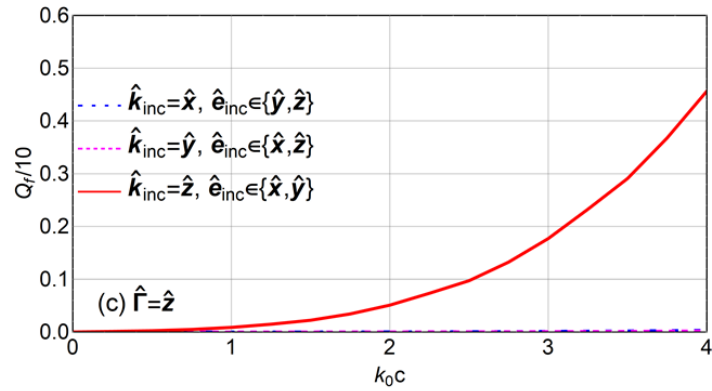
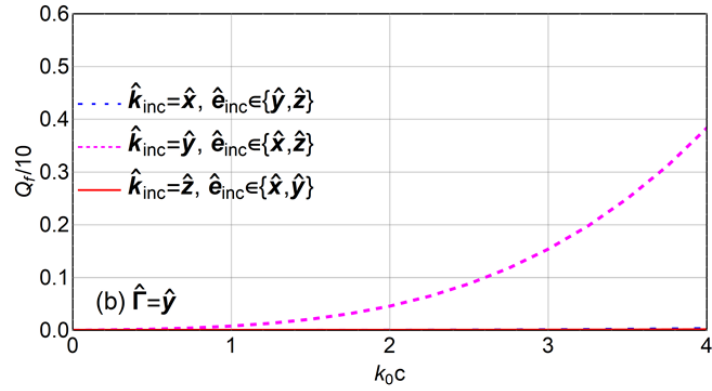
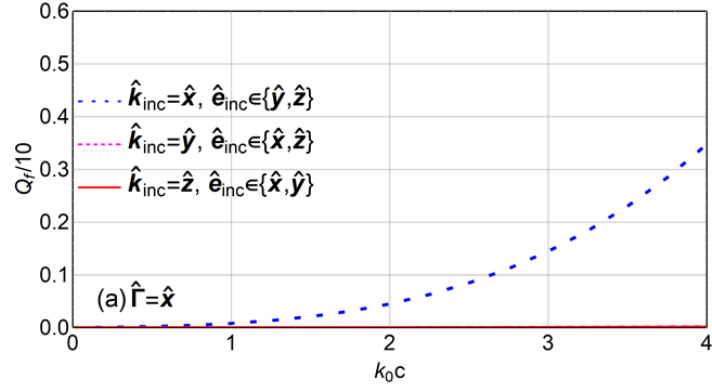


Figure 8: Same as Fig. 6, except for Q_f .